Final Draft
of the original manuscript:

Haldrup, K.; Beckmann, F.; Nielsen, S.F.; Wert, J.A..:
Experimental determination of strain partitioning among individual grains in the bulk of an aluminium multicrystal
In: Materials Characterization (2007) Elsevier

DOI: /10.1016/j.matchar.2007.07.006

Experimental determination of strain partitioning among individual grains in the bulk of an aluminium multicrystal

K. Haldrup [a,*], F. Beckmann [b], S. F. Nielsen [c] and J. A. Wert [a,c]

[a] *Metal Structures in 4D, Materials Research Department, RisøNational laboratory/ DTU, Frederiksborgvej 399, 4000, Roskilde Denmark*

[b] *GKSS-Research Center Geesthacht, 21502 Geesthacht, Germany*

[c] *Materials Research Department, RisøNational laboratory/ DTU, Frederiksborgvej 399, 4000, Roskilde Denmark*

Abstract

A recently developed marker-based technique for mapping of the Displacement Gradient Tensor and the strain throughout the bulk of optically opaque specimens is presented and applied to an aluminium alloy multicrystal. Through investigations at 4%, 10% and 14% axial strain, the internal strain field is observed to be non-homogenous with the observed patterns present throughout the range of strains investigated. The morphology of the strain field is visualized with a resolution better than 50μm and variations are tentatively associated with the grain structure as recorded by EBSD. Future applications of the technique in combination with other 3-dimensional approaches are discussed with respect to comparison with Finite-Element modelling approaches.

Key words: Polycrystal Plasticity, Strain, Non-destructive, Bulk, Tomography

PACS:

1 Introduction

How strain is partitioned among the individual crystallographic grains in a polycrystal subjected to deformation has been a long-standing problem in Materials Mechanics. Early work by Taylor and Elam [1] laid the foundation for a sound understanding of how single crystals deform, allowing Sachs [2] to propose the first polycrystal deformation model; a model prescribing only the strain along the tensile direction, leaving all other components to vary from grain to grain. This introduces the problem of strain compatibility in polycrystalline metals, since grains no longer fit together as an ensemble. The physical flaw inherent in the Sachs model is directly addressed in the model proposed by Taylor [3]. Based on observations of how grains deformed in wire drawing, this model postulated that the strain state of each individual crystallographic grain was identical to the macroscopic strain. Bishop and Hill [4] developed a similar polyslip model that was later shown to be based on assumptions equivalent to the original Taylor model [5,6]. While the Taylor-type assumptions and models were very successful in many respects, experimental results indicate that actual deformation processes in polycrystals develop heterogeneous orientation and strain [7,8] and overprediction of the sharpness of FCC textures also indicates a need for modifications. Many attempts have been made to propose such models, importantly relaxed-constraints models

* Corresponding author, email: kristoffer.haldrup@risoe.dk, phone: +45 3532 0393, fax: 4677 5758. Present address: Center for Molecular Movies, Niels Bohr Institute, H. C. rsted Institute, Universitetsparken 5, 2100 Copenhagen, Denmark

[9–11] and self-consistent models [12–15] focusing on the average properties, notably texture, of polycrystalline ensembles and Finite Element-type models [16–22] dealing in a more explicit manner with the local response, sometimes based on direct modelling of observed microstructures [23,24].

Experiments dealing with the dynamics of deformation of grain ensembles (multicrystals, polycrystals) can be broadly classified into two groups, one mostly concerned with the average response and one with the local response as well as interactions between grains. To the former belong the vast range of investigations of deformation textures as well as studies of lattice strains, both of which have been studied throughout the bulk of solid samples with penetrating radiation, e.g. neutrons or x-rays. In the latter group, experiments have been mostly concerned with two types of local observables; the local plastic strain and the local lattice orientation evolution during the course of deformation with both of these supplemented by many years of TEM investigations of deformation structures and substructures.

Regarding the direct measure of the deformation dynamics on the grain scale, local plastic strain, efforts have focused mainly along two directions, fiducial markers and Digital Image Correlation. The use of fiducial markers to infer the strain during deformation is a well-established technique since some of the earliest quantitative deformation experiments [1] and has seen a steady increase in accuracy and resolution. Using fiducial marker lines deposited by electron beam lithography [25,26], Hoc et al. [20] investigated the inter- and intra-granular strain and orientation fields on a fine scale – 2.5 - 20 μm – using specimens machined from IF-Ti steel polycrystals with varying grain sizes. Comparison of the experimental data with FE simulations allowed the authors to identify a material model incorporating non-linear hardening as superior

to linear-hardening models based on the ability of each model to reproduce the significant strain field heterogeneity that was observed experimentally. Quantified through the width of the distribution function for the tensile strain, heterogeneity was observed to saturate between 2.5% and 7.5% for this BCC specimen, an observation that could not be captured by any of the material models investigated.

In recent years, Digital Image Correlation methods by which the local strain field is inferred by comparing digital images [27,28], have also been used to obtain strain fields on a local scale on the surface of deformed polycrystals. By using SEM images for the strain measurements and Electron Back-Scatter Diffraction (EBSD) for orientation determination, it is possible to monitor both crystal orientation and plastic strain at the same time during in-situ straining experiments as presented by Sachtleber et al. [29] and Tatschl and Kolednik citetatschl03. Sachtleber et al. investigated commercial purity aluminium with columnar, mm-sized grains deformed in plane strain compression to thickness reductions corresponding to 3%, 8% and 15% engineering strain. Local plastic strain and local crystal orientation were measured with a spatial resolution of 100 μm between deformation steps. Mapping of accumulated von Mises strain, ε_{vM}, and engineering shear on one transverse surface revealed variations delineating large-angle grain boundaries and also revealed large intra-grain heterogeneities. Differences between 1% and 16% maximum ε_{vM} occur between grains, and an almost-as-large spread can be found within individual grains. Shear components of the strain were found to reflect the boundary conditions of the applied deformation. In the very detailed study by Tatschl and Kolednik, an OFHC Cu polycrystal with 100-μm grain size and a cross section of 2×2mm was deformed in tension to macroscopic strains of

7.4% and 14%. Local crystal orientation and strain were measured simultaneously on one surface of the specimen and although only strain and lattice orientation maps for 7% deformation were presented, results for 14% were reported to be qualitatively similar. Spatial resolution in this study was on the order of a micrometer and results similar to those discussed above were obtained, e.g. large inter- and intragranular variation in the measured strain fields. Also intense in-plane rotations near some boundaries were observed and the full set of orientation and strain field measurements allowed the authors to perform a Taylor-type analysis to infer slip system activity. This led to the conclusion that in most regions, only three slip systems were active as required by near-surface Taylor constraints.

While the studies mentioned above and others have advanced the field of polycrystal deformation mechanics very considerably, a significant issue has been the degree to which studies of surface behaviour are representative of the bulk [30]. This has been addressed in Finite Element simulation studies (c.f. [31–33]), but it is still uncertain exactly to which degree free surfaces perturb the local mechanical response. Experimentally, attempts to avoid complications have involved the use of split-sample techniques [17] and post-mortem sectioning [34], although the latter makes studies of orientation and structure evolution difficult. To investigate grain-scale dynamics in further detail, it is therefore highly desirable to be able to non-destructively probe crystal orientations as well as strain and stress fields on a local scale with high resolution. Diffraction-based techniques utilizing hard x-rays [35,36] or neutrons [15] to probe the evolution of crystal orientations and elastic strains throughout the bulk of optically opaque samples have emerged over the past few years, but local plastic strain fields caused by macroscopic deformation cannot currently be

obtained via these methods. Instead, researchers have applied classic methods for strain measurements as those discussed in section above to tomographic reconstructions of the 3D structure of metallic specimens, using both Digital Image Correlation [37,38] and marker particles, [39–43] to infer the local, plastic strain fields throughout the bulk optically opaque, but x-ray transparent, specimens.

It is the purpose of the present article to present and apply the marker-based method described in detail by Haldrup et al. [43] to assess the distribution of plastic strain on the scale of individual grains throughout the bulk of a metallic specimen. To do so, an Al+W alloy multicrystal with columnar grain structure has been deformed in compression to an engineering strain of 14% in three steps, between which the position of 30,000 internal W markers has been recorded by synchrotron x-ray micro-tomography.

2 Experimental method

For these experiments, Al samples containing W marker particles were prepared by a powder-metallurgical route described in detail in [39]. In outline, it is based on mechanical mixing of Al and W powders with the latter constituting about 1 vol% of the mix, followed by cold compaction and hot extrusion to form a void-free stock material with a density equal to that calculated based on rule-of-mixtures. The W and Al marker particles used for this study were on average 10 μm in diameter and total marker particle content was slightly over 1% by volume.

For characterization of the deformation field inside specimens made from this

2-phase alloy, synchrotron x-ray micro-tomography is used to record the position and shape of each marker particle in 3D before and after deformation. Using the morphologies of individual W particles, the markers can then be uniquely identified in both data sets and their displacement during deformation can be found. From these measurements, the displacement vectors $\mathbf{u}$ of individual markers can be followed and the displacement gradient tensor (DGT) field $\tilde{\mathbf{f}}$ defined as

$$\tilde{\mathbf{f}} = e_{ij} = \frac{\partial u_i}{\partial x_j} = \begin{pmatrix} \frac{\partial u_1}{\partial x_1} & \frac{\partial u_2}{\partial x_1} & \frac{\partial u_3}{\partial x_1} \\ \frac{\partial u_1}{\partial x_2} & \frac{\partial u_2}{\partial x_2} & \frac{\partial u_3}{\partial x_2} \\ \frac{\partial u_1}{\partial x_3} & \frac{\partial u_2}{\partial x_3} & \frac{\partial u_3}{\partial x_3} \end{pmatrix} \tag{1}$$

can subsequently be derived by calculation of the partial derivatives with respect to nearest neighbours, as described in detail in [43] where a full description of the methodology used for these experiments is presented. Spatial resolution is directly related to the density of marker particles and – quantified in terms of the width of the trace of the DGT – strain resolution is better than 0.01 (1%) in most cases.

For the deformation experiments, polycrystalline samples were obtained by a two-step drawing/annealing sequence of the extruded 6 mm stock material, giving a final diameter of 2 mm. The resulting grain structure was irregular with columnar grains with a typical transverse grain dimension on the order of 100-200 μm. From this material, cylindrical compression specimens 1mm in diameter and 1.75mm in height were machined. Figure 1 shows the end-face grain structure (obtained by EBSD) superimposed on a micrograph of the specimen after deformation. Also shown is an SEM micrograph of the sample

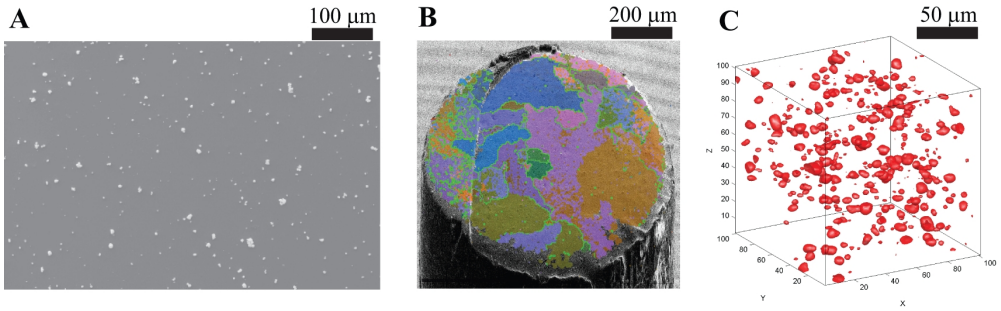

Fig. 1. **A**: Micrograph of the sample surface with individual markers clearly visible. **B**: SEM micrograph of the polished sample end after deformation - an interpolated (to avoid holes at markers) EBSD scan showing the grain structure is superimposed. **C**: A 3D rendering of the tomographic reconstruction showing individual markers. Note the differences in W particle morphologies that are used for tracking.

surface clearly showing the markers and a tomographic reconstruction with the matrix material removed so the markers are visible.

Compression experiments were performed with a small screw-driven compression rig at an initial strain rate of $\dot{\varepsilon} = 2 * 10^{-3} s^{-1}$ without lubrication of the end platens. Deformation of the sample was performed ex-situ from the tomography equipment such that four levels of deformation were applied, 0%, 4%, 10% and 14% engineering strain, and after each a tomographic recording of the sample volume was acquired. Reconstruction of the local absorption-intensity in the sample volume was performed by a standard Fourier back-projection scheme giving a reconstructed voxel size of 1.5 μm and point-point resolution of slightly under 3μm. 256 gray levels represent the local absorption intensity in the reconstructed volume. The experiment was carried out at beamline BW2 at HASYLAB/DESY in Hamburg at an x-ray energy of 24 keV, see [44,45] for a description of the beamline and tomography equipment.

By thresholding and segmentation of the reconstructed volumes, 75,000 W

marker particles were detected in each tomogram. Based on individual particle morphology, marker particles were tracked between deformation steps using tracking and refinement algorithms presented in detail in [43] with a yield of 50-60%, giving a total of 35,000 tracked markers for the first two deformation levels and 23,000 for the last. From the positions of these markers before and after deformation, the local displacement field can be found with sub-pixel accuracy and a spatial resolution of slightly above 30 μm determined by the nearest-neighbour distance.

3 Results

Turning first to the displacement field from which the DGT field and strain are derived, Figure 2 shows displacement vectors in a vertical section through the center of the specimen at 4%, 10% and 14% strain. This also introduces the coordinate system used: in all cases positions are referred to the original, undeformed condition of the sample. Although the displacement field appears fairly homogenous, heterogeneities are visible at the higher strain levels, especially for sections orthogonal to the compression axis.

To quantify these inhomogeneities, the DGT is calculated from the flow field for all three levels of deformation. Figure 3 shows the distribution functions for each of the e_{ij}-components arranged as the corresponding e_{ij}-tensor. The distributions for each deformation step have been normalized to the applied strain defined as the mean strain along the 3-direction, e_{33}. The slight broadening of the distribution at 4% is due to the experimental resolution being close to the applied strain, but otherwise the shape of the distribution functions appears to be relatively unaffected by the strain level. This is also the case for

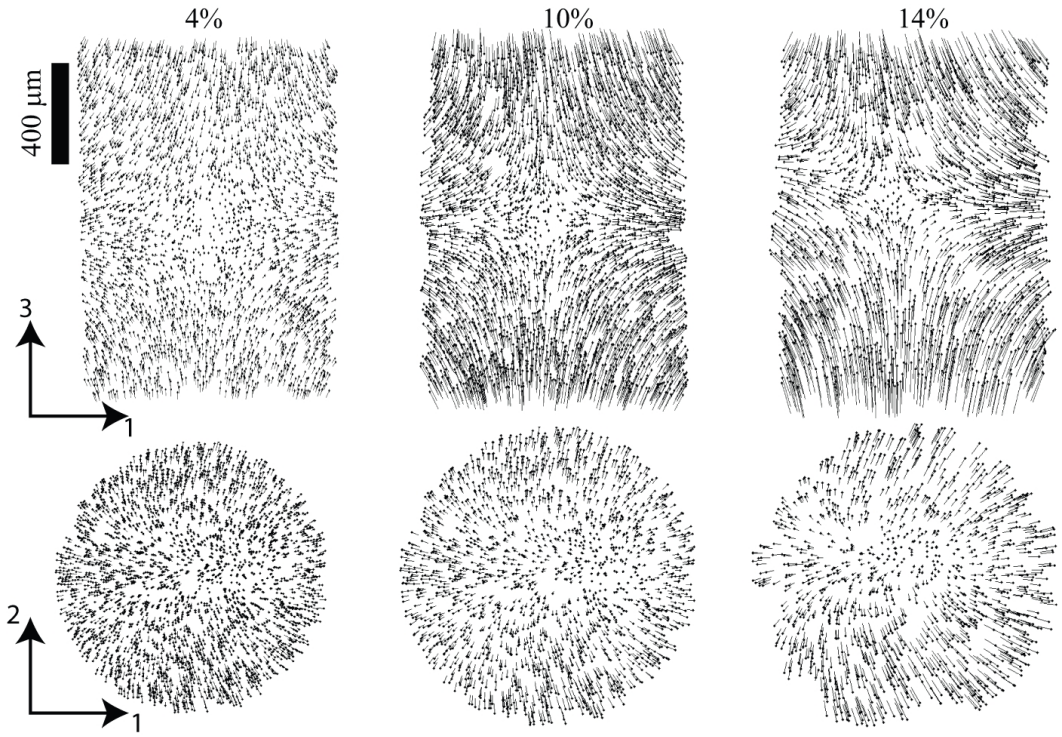

Fig. 2. Displacement vectors identified by the marker tracking procedure. 3 levels of strain are shown with the heterogeneity of the displacement field becoming more evident with increasing deformation.

the e_{12}-component, although the bimodality is blurred by the experimental resolution at 4% axial strain. Resolution of this measurement is quantified in terms of 1/3 the width of the trace of the DGT (from conservation of volume) Figure 3b shows it to increase from better than 0.01(1% strain) at 4% macroscopic deformation to almost 0.03 for 14 % macroscopic deformation although it remains almost constant relative to the applied macroscopic deformation.

Relating the properties of a 9-component tensor to a series of points in 3-space and as a function of strain (or time) in a convenient and readily understandable form is challenging [46], but Figure 5 illustrates one method by presenting virtual slices perpendicular to the loading direction. DGT-component values in 225 μm thick slices are translated onto a square grid with a resolution of 30

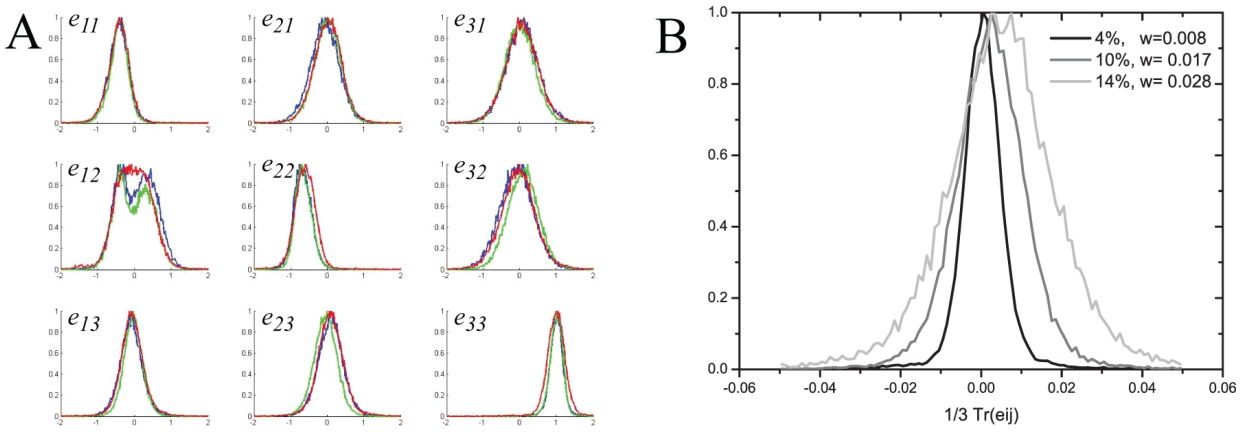

Fig. 3. **A**: Normalized distribution functions for each individual component of the Displacement Gradient Tensor for the three strain levels – red is 4%, green is 10% and blue is 14%. Deviations from homogeneity are evident for several of the components for all three levels of strain, which does not seem to influence the shape of the distributions. B: The distribution function for the trace of the Displacement Gradient tensor at the three strain levels. The width quantifies the accuracy of the measurement of the individual components of the tensor.

pixels (45 μm). For comparison, the same data are represented by two color scales, one defined by the axial strain of the most recent deformation increment (top row) and one by the maximum applied strain during the experiment (bottom row). From this, the overall increase in strain is evident but also the fact that the structural features of the strain field appear largely unchanged by the level of imposed strain. In the following, focus will be on the dataset representing 10% axial compression and unless explicitly stated, the results presented are equivalent for all three axial strain levels.

Examining the 10% dataset in more detail, Figure 5 shows sections through the top, middle and bottom of the reconstructed volume as well as sections perpendicular to the "1" and "2" axes. The features present, including the

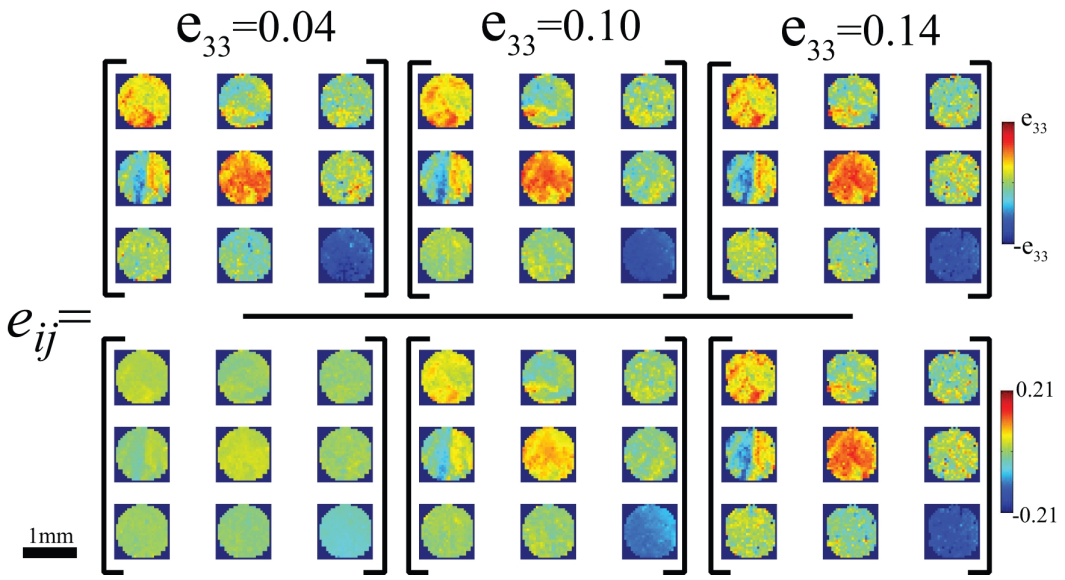

Fig. 4. Sections through the specimen center, showing how the increase in applied strain intensifies the structures of the strain field while the morphology stays the same. Two color scales for the same data are shown.

prominent bimodal "swirl" structure of the e_{12}-component, appear to extend along the entire specimen height as would be expected from the columnar grain structure.

To illustrate how the calculated displacement gradient tensor contains all information regarding the deformation of the specimen and to separate the measured plastic strain from any rigid-body rotations, Figure 6 shows the displacement gradient tensor for the mid-section of the sample along with the strain $\epsilon = \frac{1}{2}(e_{ij} + e_{ji})$ and the rotation $\omega = \frac{1}{2}(e_{ij} - e_{ji})$.

The complex nature of the observed strain field can be further illustrated by 3-dimensional rendering of strain field iso-surfaces. Figure 7 shows this with two values of iso-surface threshold, one highlighting deviations from homogenous deformation for the diagonal components and one highlighting deviations for the off-diagonal components.

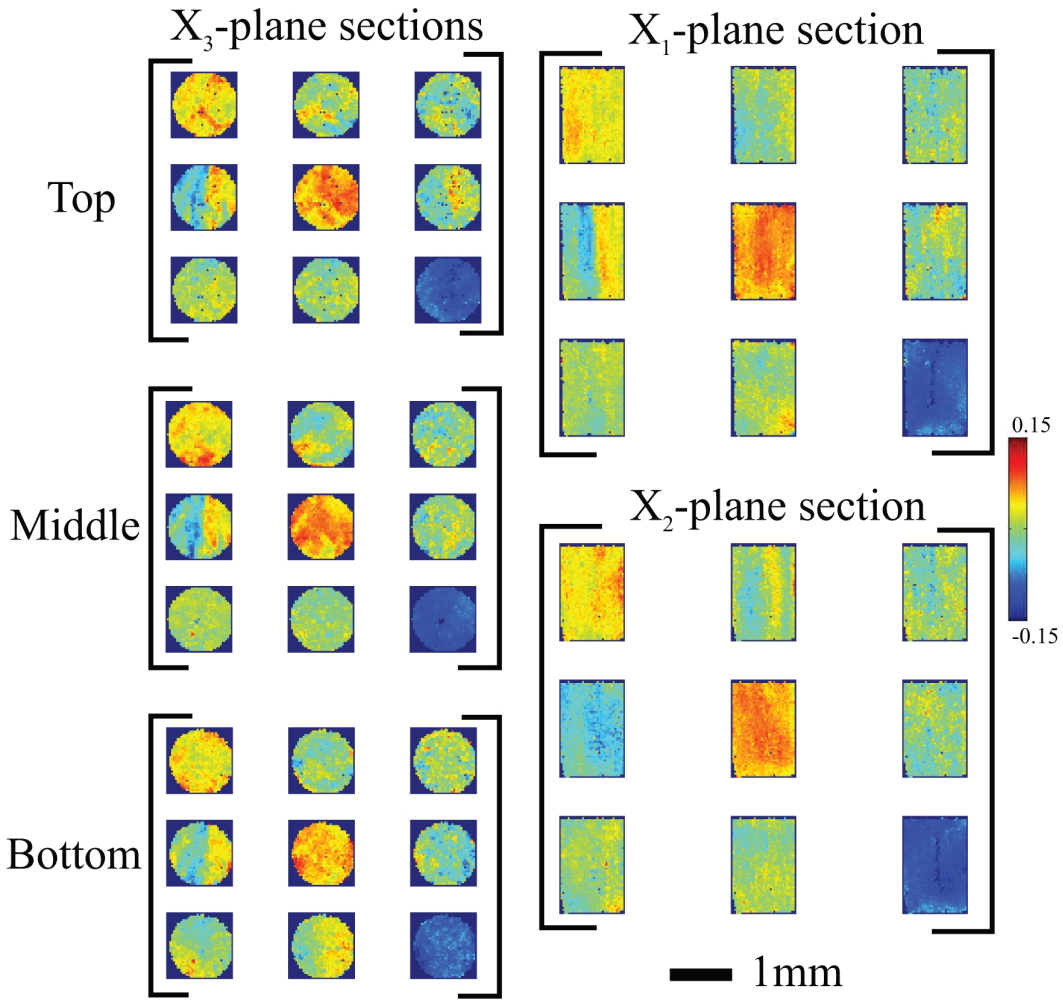

Fig. 5. 225μm-sections through the sample near the top, middle and bottom planes. Also shown are vertical sections, with the elongated structure of the grains evident. In both Figure 4 and 7, the columnar nature of the grain structure in this specimen is reflected in the elongated nature of the strain distributions.

4 Discussion

In the preceding section, data were presented for the locally measured plastic strain (actually, the displacement gradient tensor field) in an Al-alloy multicrystal deformed in compression. Initially disregarding spatial information,

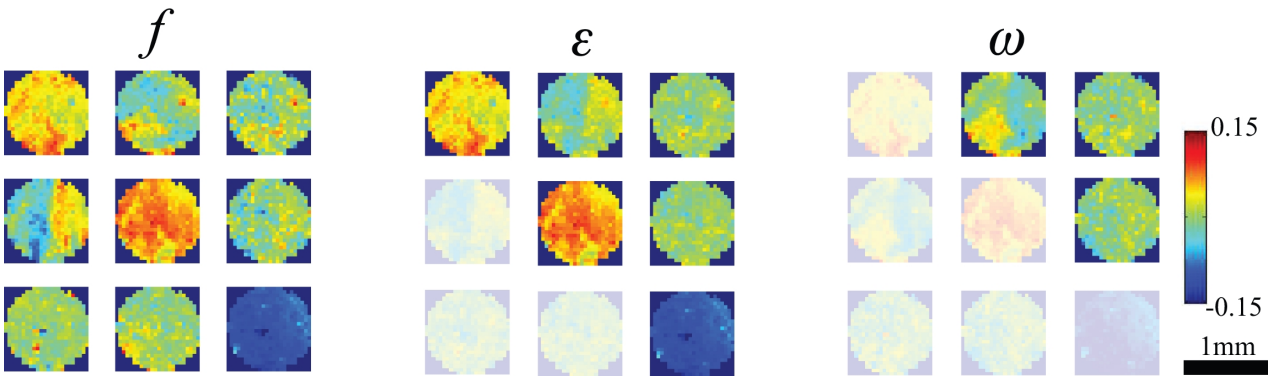

Fig. 6. Three representations of the data on a slice through the central part of the specimen. From left to right are shown the Displacement Gradient Tensor, the Strain tensor and the Rotation tensor. Note how the off-diagonal components exhibit a complex combination of shear and rotation.

Figure 3 shows the distribution functions for each component of the DGT for the 4%, 10% and 14% engineering strain along the compression direction. The shape of these distribution functions are to a very good approximation Gaussian and we ascribe this form of the distributions to intrinsic variations in sample response in agreement with the modelling results reported by Sarma and Dawson [48], as the uncertainty in determining the components of f is known to follow a Lorentzian distribution function [43].

In agreement with Hoc et al. [20], we observe no changes in the shape of these distributions with increasing strain but for the component parallel to the deformation direction, the width observed in this study is somewhat smaller (about 0.4 compared with 1 (estimated)) and we do not observe any bimodality. This indicates that either this feature disappears between the 2% strain level where it was observed in [20] and the first strain level presented here, 4%, or it is a feature peculiar to the experiment performed by those investigators; their experiment and the one presented here differ in several important details and differences would not be unexpected.

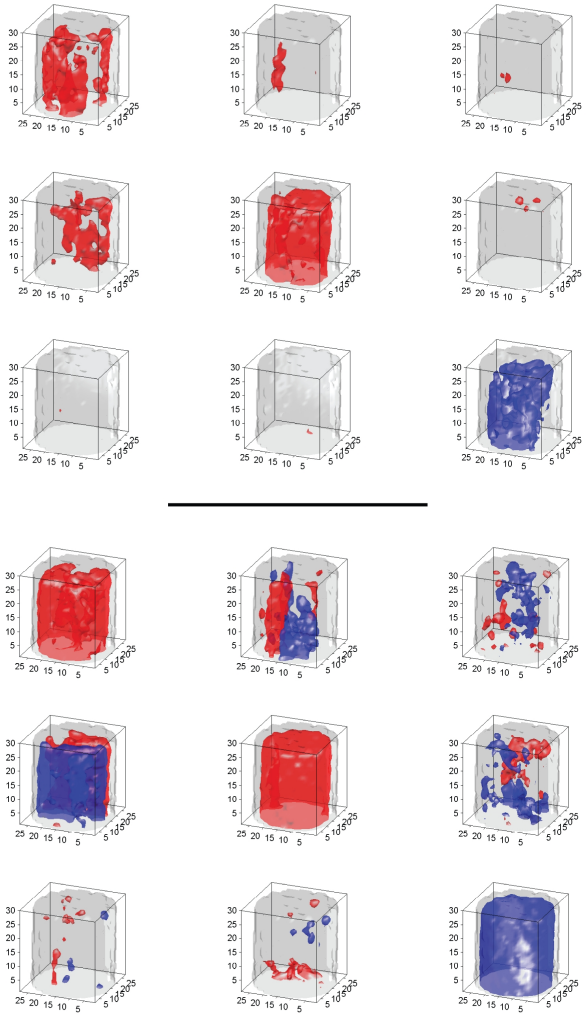

Fig. 7. 3-dimensional representations of Displacement gradient tensor iso-surfaces. Top figure is with a high thresholds(red=0.05, blue=-0.1) to illustrate the spatial distribution of high strain for the diagonal components while the lower figure is with thresholds at ±0.02 to show deviations from homogeneity for the off-diagonal components.

Turning to the locally resolved observations, Figure 4 further illustrates the point of strain similarity regardless of strain level but also clearly shows how the strain field is spatially heterogeneous within this specimen. Focusing next on the 10% deformation step, Figure 4 shows the spatial distribution of strain

on selected sections through the sample volume. Heterogeneities in the strain field are observed to be present on several length scales, ranging from the sample scale where effects of friction are seen as lowering of the strain level near the sample ends, which are in direct un-lubricated contact with the compression rig platens.

On a finer scale, the heterogeneity of the strain field is seen to be quite complex. For the normal components, strain can be partitioned among the e_{11}, e_{22} and e_{33} under the requirement of volume conservation, i.e. the trace must be zero. As a consequence, the compressive strain is observed to be fairly homogenous as the required reduction in height can only be accommodated by a change in length along one dimension, whereas the transverse components show larger variability as the required widening of the specimen can be by a combination of two transverse strains. These observations of more highly localized transverse strains are in agreement with the surface study presented by Tatschl and Kolednik [47] and the same effects are reflected in the distributions of the off-diagonal components of ϵ and ω.

The present description does not include preliminary EBSD measurements of the crystal orientation of the surface of the investigated sample and the fairly complex grain structure precludes direct association of features in the strain maps with the crystallographic orientation of individual grains. However, the length scale of the heterogeneities in the observed strain field as seen e.g. in Figure 5 is commensurate with the size of some of the larger grains as determined by EBSD. Additionally, the elongated geometry of the strain field iso-surfaces is in good agreement with the columnar nature of the grain structure in this sample.

On a general level, it is uncertain whether it would be possible to determine the location of grain boundaries from the present data without complementary information from measurements of the local lattice orientation as in [29] and [47]. Overall morphologies of the observed strain fields appear alike in those studies as well as the present investigation, with a combination of grain-scale variation and regions of concentrated strain, in the latter case often at or across grain boundaries and triple junctions. The three-dimensional structure of these effects should become clear with further experiments, using the capability of the technique presented here to test this in the bulk for the first time. In combination with new techniques for measuring the local crystal orientations throughout the bulk [35,36,49], new opportunities present themselves for rigorous testing of (poly)crystal plasticity theories and models through the direct comparison with locally resolved simulations.

5 Conclusions

In the preceding sections, a new technique utilizing a dispersion of marker particles to measure the 3-dimensional distribution of local plastic strain has been demonstrated for the first time on a coarse-grained metallic material. An aluminium alloy containing such markers has been recrystallized to form large, columnar grains and has been deformed to 14% in uniaxial compression. The internal strain field has been found to deviate significantly from the homogenous response reported in the first application of the marker-based technique on a similar, but fine-grained sample. The present investigation has a spatial resolution of slightly above 30 μm, less than the average grain size, and data indicate that the deviations from homogeneity are related to the

grain structure of the multicrystal as well as neighbour interactions, but this has not been proven. Further work will aim to directly associate the local crystal orientation with the local strain field and to employ this information in investigations of polycrystal plasticity.

6 Acknowledgements

The authors would like to gratefully acknowledge Palle Nielsen and Preben Olesen for technical support and Henning F. Poulsen for valuable discussions. We acknowledge the Danish National Research Foundation for supporting the Center for Fundamental Research: Metal Structures in Four Dimensions. Additional support was provided by the Danish Natural Science Research Council (via Dansync)

References

[1] G. I. Taylor, C. F. Elam, The distortion of an aluminium crystal during a tensile test, Proceedings of the Royal Society, Bakerian Lecture 102 (1923) 643.

[2] G. Sachs, Zur ableilung einer fliessbedingung, VDI Z 72 (1928) 734.

[3] G. I. Taylor, plastic strain in metals, Journal of the Institute for Metals 62 (1938) 307.

[4] J. F. W. Bishop, R. Hill, A theory of plastic distortion of a polycrystalline aggregate under combined stresses, Philosophical Magazine 42 (1951) 414.

[5] G. Y. Chin, W. L. Mammel, Generalization and equivalence of the minimum work –taylor– and maximum work –bishop-hill– principles for crystal plasticity,

Transactions of the metallurgical Society A.I.M.E. 245 (1969) 1211–1214.

[6] U. F. Kocks, Metallurgical Transactions 1 (1970) 1121–1143.

[7] C. Barrett, L. Levenson, Structure of aluminium after compression, Transactions of AIME 135 (1940) 327–352.

[8] W. Boas, M. E. Hargreaves, On the inhomogeneity of plastic deformation in the crystals of an aggregate, Proceedings of the Royal Society of London A 193 (1947) 89–97.

[9] T. Leffers, Computer simulation of the plastic deformation in faced centered cubic polycrystals and the rolling texture derived, in: RisœReport R184, ICOTOM 1, 1968.

[10] H. Honeff, H. Mecking, A method for the determination of the active slip systems and orientation changes during single crystal deformation, in: G. Gottstein, K. Lucke (Eds.), 5th ICOTOM, Springer, 1978.

[11] U. Kocks, G. Canova, in, Deformation of Polycrystals, Eds. N. Hansen, A. Horsewell, T. Leffers, H. Lilholt, Risoe National Laboratory (1981) 35–44.

[12] E. Kroner, Zur plastichen verformerung des vielkristalls, Acta metallurgica 9 (1961) 155–161.

[13] J. W. Hutchinson, Proceedings of the Royal Society of London A 319 (1970) 247.

[14] A. Molinari, G. Canova, S. Ahzi, A self-consistent approach of the large deformation polycrystal viscoplasticity, Acta Metallurgica 35 (1987) 2983–2994.

[15] B. Clausen, T. Lorentzen, T. Leffers, Self-consistent modelling of the plastic deformation of f.c.c. polycrystals and its implication for diffraction measurements of internal stresses, Acta Materialia 46 (1998) 3087–3098.

[16] A. Needleman, R. Asaro, J. Lemonds, D. Peirce, Finite-element analysis of crystalline solids, Computer Methods In Applied Mechanics And Engineering 52 (1985) 689–708.

[17] S. Panchanadeeswaran, R. D. Doherty, R. Becker, Direct observation of orientation change by channel die compression of polycrystalline aluminum-use of a split sample, Acta Materialia 44 (1995) 1233–1262.

[18] A. Beaudoin, H. Mecking, U. Kocks, Development of localized orientation gradients in fcc polycrystals, Computer Methods In Applied Mechanics And Engineering 73 (1996) 1503–1517.

[19] F. Delaire, J. L. Raphanel, C. Rey, Plastic heterogeneities of a copper multicrystal deformed in uniaxial tension: experimental study and finite element simulations, Acta Materialia 48 (2000) 1075–1087.

[20] T. Hoc, J. Crepin, L. Gelebart, A. Zaoui, A procedure for identifiyng the plastic behaviour of single crystals from the local response of plycrystals, Acta Materialia 51 (2003) 5477–5488.

[21] P. Erieau, C. Rey, Modeling of deformation and rotation bands and of deformation induced grain boundaries in if steel aggregate during large plane strain compression, International Journal of Plasticity 20 (2004) 1763–1788.

[22] S. R. Kalidindi, A. Bhattacharyya, R. D. Doherty, Detailed analyses of grain-scale plastic deformation in columnar polycrystalline aluminium using orientation image mapping and crystal plasticity models, Proceedings of the Royal Society of London A 460 (2004) 1935–1956.

[23] R. Becker, Analysis of texture evolution in channel die compression - i. effects of grain interaction, Acta Metallurgica et Materialia 39 (1991) 1211–.

[24] R. Becker, S. Panchanadeeswaran, Effects of grain interactions on deformation and local texture in polycrystals, Acta Metallurgica 43 (1995) 2701–2719.

[25] D. G. Attwood, P. M. Hazzledine, A fiducial grid for high-resolution metallography, Metallography 9 (1976) 483–501.

[26] L. Allais, M. Bornert, T. Bretheau, D. Caldemaison, Experimental characterization of the local strain field in a heterogeneous elastoplastic material, Acta metallurgica et materialia 42 (1994) 3865–3880.

[27] J. Q. D. Fonseca, P. Mummery, P. J. Withers, Full-field strain mapping by optical correlation of micrographs acquired during deformation, Journal of Microscopy 218 (2005) 9–21.

[28] F. Lagattu, J. Brillaud, M.-C. Lafarie-Frenot, High strain gradient measurements by using digital image correlation technique, Materials Characterization 53 (2004) 17–28.

[29] M. Sachtleber, Z. Zhao, D. Raabe, Experimental investigation of plastic grain interaction, Materials Science and Engineering A 336 (2002) 81–87.

[30] S. Miyazaki, K. Shibata, H. Fujita, Effects of specimen thickness on mechanical properties of polycrystalline aggregates with various grain sizes, Acta Metallurgica 27 (1978) 855–862.

[31] T. E. Buchheit, R. J. Bourciery, G. W. Wellmanz, M. K. Neilsenz, Capturing the influence of surface constraints in small and thin samples using polycrystalline plasticity theory, Modelling and Simulations in Materials Science and Engineering 5 (1997) 421–437.

[32] G. Cailletaud, S. Forest, D. Jeulin, F. Feyel, I. Galliet, V. Mounoury, S. Quilici, Some elements of microstructural mechanics, Computational Materials Science 27 (2003) 351–374.

[33] K. Haldrup, R. D. McGinty, D. L. McDowell, Effects of constraints on lattice orientations and strain in polycrystal plasticity simulations, Submitted to Materials Science and Engineering A.

[34] N. Zaafarani, D. Raabe, R. Singh, F. Roters, S. Zaefferer, Three-dimensional investigation of the texture and microstructure below a nanoindent in a cu single crystal using 3d ebsd and crystal plasticity finite element simulations, Acta Materialia 54 (2006) 1863–1876.

[35] H. F. Poulsen, S. F. Nielsen, E. M. Lauridsen, S. Schmidt, R. M. Suter, U. Lienert, L. margulies, T. Lorentzen, D. J. Jensen, Three-dimensional maps of grain boundaries and the stress state of individual grains in polycrystals and powders, Journal of Applied Crystallography 34 (2001) 751–756.

[36] B. Larson, W. Yang, G. Ice, J. D. Budai, J. Tischler, Three-dimensional x-ray structural microscopy with submicrometre resolution, nature 415 (2002) 887–890.

[37] B. K. Bay, T. S. Smith, D. P. Fyhrie, M. Saad, Digital volume correlation: Three-dimensional strain mapping using x-ray tomography, Experimental Mechanics 39 (1999) 217–226.

[38] E. Verhulp, B. van Rietbergen, R. Huiskes, A three-dimensional image correlation technique for strain measurements in microstructures, Journal of Biomechanics 37 (2004) 1313–1320.

[39] S. Nielsen, H. Poulsen, F. Beckmann, C. Thorning, J. Wert, Measurements of plastic displacement gradient components in three dimensions using marker particles and synchrotron x-ray absorption microtomography, Acta Materialia 51 (2003) 2407–2415.

[40] H. Toda, I. Sinclair, J.-Y. Buffiere, E. Maire, K. Khor, P. Gregson, T. Kobayashi, A 3d measurement procedure for internal local crack driving forces via synchrotron x-ray radiation, Acta Materialia 52 (2004) 1305–1317.

[41] K. Haldrup, S. F. Nielsen, F. Beckmann, J. A. Wert, Inhomogeneous plastic flow investigated by x-ray absorption micro-tomography of an aluminium alloy

containing marker particles, Journal of Microscopy 222 (2006) 28–35.

[42] T. Ohgaki, H. Toda, M. Kobayashi, K. Uesugi, M. Niinomi, T. Akahori, T. Kobayash, K. Makii, Y. Aruga, In situ observations of compressive behaviour of aluminium foams by local tomography using high-resolution x-rays, Philosophical Magazine 86 (2006) 4417–4438.

[43] K. Haldrup, S. F. Nielsen, J. A. Wert, A methodology for full-field plastic strain measurements using x-ray absorption tomography and internal markers, Submitted to Experimental Mechanics.

[44] W. Drube, H. Schulte-Schrepping, H.-G. Schmidt, R. Treusch, G. Materlik, Design and performance of the high-flux/high-brightness x-ray wiggler beamline bw2 at hasylab, Review of Scientific Instruments 66 (1995) 1668–1670.

[45] F. Beckmann, T. Donath, J. Fischer, T. Dose, T. Lippmann, L. Lottermoser, R. V. Martins, A. Schreyer, New developments for synchrotron-radiation-based microtomography at desy, in: Proceedings of SPIE06, Developments in x-ray tomography V, 2006.

[46] B. Jeremic, G. Scheuermann, J. Frey, Z. yang, B. Hamann, kenneth I. joy, H. Hagen, Tensor visualizations in computational geomechanics, International journal for numerical and analystical methods in geomechanics 26 (2002) 925–944.

[47] A. Tatschl, O. Kolednik, A new tool for the experimental characterization of micro-plasticity, Materials Science and Engineering A 339 (2003) 265–280.

[48] G. Sarma, P. R. Dawson, Effects of Interactions among Crystals on the Inhomogenous Deformations of Polycrystals, Acta Materialia (1996) 1937–1953

[49] G. Winther, L. Margulies, S. Schmidt, H. Poulsen, Lattice rotations of individual bulk grains part ii: correlation with initial orientation and model comparison, Acta Materialia 44 (2004) 2863–2872.